

Article

## Nonintrusive Energy Monitoring for Microgrids Using Hybrid Self-Organizing Feature-Mapping Networks

Ying-Yi Hong \* and Jing-Han Chou

Chung Yuan Christian University, 200 Chung Pei Road, Chung Li 320, Taiwan;

E-Mail: caroter83@yahoo.com.tw

\* Author to whom correspondence should be addressed; E-Mail: yyhong@dec.ee.cycu.edu.tw;  
Tel.: +886-3-2654050; Fax: +886-3-2654059.

Received: 3 May 2012; in revised form: 11 July 2012 / Accepted: 12 July 2012 /

Published: 18 July 2012

---

**Abstract:** Microgrids can increase power penetration from distributed generation (DG) in the power system. The interface (*i.e.*, the point of common coupling, PCC) between the microgrid and the power utility must satisfy certain standards, such as IEEE Std. 1547. Energy monitoring of the microgrid at the PCC by the power utility is crucial if the utility cannot install advanced meters at different locations in the microgrid (e.g., a factory). This paper presents a new nonintrusive energy monitoring method using a hybrid self-organizing feature-mapping neural network (SOFMNN). The components of the FFT spectra for voltage, current, kW and kVAR, measured at the PCC, serve as the signatures for the hybrid SOFMNN inputs. The nonintrusive energy monitoring at the PCC identifies different load levels for individual linear/nonlinear loads and output levels for wind power generators in the microgrid. Using this energy monitoring result, the power utility can establish an energy management policy. The simulation results from a microgrid, consisting of a diesel generator, a wind-turbine-generator, a rectifier and a cyclo-converter, show the practicability of the proposed method.

**Keywords:** microgrid; nonintrusive energy monitoring; harmonics; self-organizing feature mapping

---

## 1. Introduction

Renewable energies, such as solar, wind, geothermal, biomass, tidal, and hydropower, are classified as distributed electricity resources and have recently been the subject of much attention as alternative sources of electricity. The advantages of renewable energies include a decrease in the required transmission capacity, real power loss and conventional generator expansion. Moreover, the use of renewable energies can significantly mitigate the emission of CO<sub>2</sub>, to meet the strict requirements laid out in the Kyoto Protocol [1]. However, penetration of the renewable energies in the distribution system can lead to many operational problems, e.g., protection coordination. One solution, which allows the main power grid to use the original protection coordination, is the embedding of these distributed generations in micro grids. The interface (*i.e.*, point of common coupling, PCC) between the microgrid and main power grid must satisfy certain standards, such as IEEE Sd. 1547 [2]. If the PCC cannot comply with the standard, the microgrid is not allowed to connect with the main grid.

The microgrid studied in this paper is related to a factory containing distributed generations. Monitoring of such microgrid energy at the PCC by the power utility is crucial, because the utility cannot install advanced meters at different locations in the microgrid, which is operated by the factory. Hence, the power utility must use nonintrusive energy monitoring (NEM) at the PCC. Traditionally, the utility can only know the resultant voltage, aggregated current, real power and reactive power at the PCC and does not know the patterns of individual power generations and behaviors of individual energy consumptions inside the microgrid. If the connection of a microgrid to the main grid satisfies IEEE Sd. 1547, e.g., power quality requirement, the utility can use the results obtained by the NEM to make further decisions. Details on the purpose and benefits of the NEM can be found in Section 2.2.

Traditionally, nonintrusive monitoring is primarily used in appliance monitoring [3], using the current and voltage of the total load, as measured at the interface to the power utility. The nonintrusive monitoring estimates the number and nature of the individual appliances, their individual energy consumptions and other related statistics (e.g., time-of-use variations). This type of nonintrusive monitoring is termed nonintrusive appliance load monitoring (NALM). An example of NALM is an “*energy audit*”, which provides a report that looks like a telephone bill, with itemized charges. *Failure analysis* can be also undertaken using NALM because a failed appliance can often be detected by its abnormal power consumption. As a *security* example, NALM can be used in a vacation home, which is unoccupied for a long period. The concept of NALM is similar to that of NEM; however, there are some differences, as follows:

- (1) NEM must consider the intermittent nature of renewable energies (e.g., wind-turbine) in a micro grid; a NALM-based residential home generally does not have a power resource.
- (2) Three-phase and non-characteristic loads (e.g., cyclo-converters of varying non-integer harmonics) are becoming more popular in microgrids but most appliances are single-phase with characteristic loads (e.g., 4-pulse converters).
- (3) The purpose of NEM in a microgrid is to monitor power generation from distributed generators and power consumption by individual loads; the purpose of NALM in a residential home is to determine the energy consumption pattern of individual appliances.

To the authors' knowledge, no research papers have so far dealt with the NEM of microgrids. However, some papers have considered NALM and these can be used as references [4–7]. Leeb *et al.* proposed a current spectral preprocessor for initial use in a transient event detector and then a transient event detection algorithm was developed for a NALM using the coefficients of the Fourier series [4]. However, the Fourier series can only be used to study a periodic signal; the use of Fourier series to serve as a transient detector for NALM would seem inappropriate. Cole and Albicki presented harmonic components as a measure for NALM in [5]. The Hamming distance between the measured and known harmonic energies is mapped into a set of known individual load states [5]. Cox and Leeb *et al.* proposed a preprocessor that computes short-time estimates of the spectral content of the voltage waveform using Fourier series [6]. If an event with transients is located, the least-square-error (LSE) method is used to match the data surrounding the event to templates, known as exemplars. However, determination of weighting factors for the LSE was not discussed. Recently, Chang and Yang proposed a genetic-based neural network to allow pattern recognition for a household appliance [7]. However, a supervised neural network, incorporating a genetic algorithm, requires a long CPU time.

Artificial neural networks (ANN) can map a set of independent variables into another set of dependent variables in a nonlinear system. ANN's can be classified into two groups—supervised and unsupervised ANN's. Supervised ANN's, e.g., back-propagation-based ANN's, need pairs of input-output data to train the weighting factors in the ANN. Unsupervised ANN's, e.g., self-organizing, feature-mapping neural networks [8], play the role of a preprocessor to extract features from a nonlinear system. ANN's have been successfully used to solve many power system problems, such as wind power/speed forecasting [9], voltage stability margin estimation [10], security-constrained optimal power flow [11] and power system stability [12]. Supervised ANN's, used for stochastic optimization [9], back-propagation algorithms [10,11] and projection schemes [12], are the most popular.

This paper proposes a novel method to achieve nonintrusive energy monitoring at the PCC between the main power grid and the microgrid, based on a hybrid self-organizing feature-mapping neural network (hybrid SOFMNN). The microgrid studied in this paper is related to a factory containing linear/nonlinear loads and distributed generations. The SOFMNN serves as a preprocessor to extract the features of signatures, obtained by fast Fourier transforms (FFT). These features appear on a two-dimensional layer that is cascaded to a supervised two-layer perceptron (neural network). The proposed hybrid SOFMNN outputs the levels of individual loads and wind power generation. The advantages of the proposed method can be summarized as follows: (1) there is no transient detection [4,6] involved in the proposed method; (2) the capability for nonlinear mapping of ANN's is greater than that of the Hamming distance [5] and LSE methods [6]; (3) the CPU time required by hybrid SOFMNN is much shorter than that for genetic-based NN's [7]; and (4) FFT is used, because non-characteristic and non-periodic signals cannot be studied using Fourier series [4,5].

Section 2 provides a problem description. The proposed method for NEM is detailed in Section 3. The simulation results, obtained from a microgrid, containing a diesel generator, a wind power generator, a rectifier and a cyclo-converter, are discussed in Section 4. Concluding remarks are given in Section 5.

## 2. Problem Description

### 2.1. Microgrid

A microgrid can be a part of the distribution system, *e.g.*, industry park, community, factory, or school [13–15]. The microgrid studied in this paper is operated by a single customer, a factory containing distributed generations.

The distributed generation resources are included in the microgrid. There are three types of distributed generation resources: (1) small and modular generating systems (such as micro-turbines, diesel generators, and cogeneration of heating/power systems); (2) energy storages (such as battery); and (3) renewable energy resources (such as solar, wind, geothermal, biomass, tidal, and hydropower). Depending on local regulations, the microgrid can output electricity to the main power grid owned by the utility. Alternatively, in compliance with IEEE Std. 1547, the CERTS microgrid does not output power to the main power grid [16]. The microgrid studied in this paper includes diesel and wind-turbine-generators and there is no surplus power injected into the main grid.

In this paper, the studied microgrid is a factory and has a linear load and nonlinear loads fed by the rectifier and cyclo-converter [17]. Figure 1 illustrates the instantaneous load currents through the rectifier. The total harmonic distortion (THD) is 4.35%. Figure 2 shows the non-characteristic load current caused by the cyclo-converter. The load currents from the cyclo-converter are non-characteristic and include inter-harmonics (whose harmonic orders are within two consecutive integers) and sub-harmonics (components with frequencies smaller than the fundamental frequency). Detailed SIMULINK implementations for both rectifier and cyclo-converter are given in the appendix.

**Figure 1.** Harmonic load current caused by the rectifier.

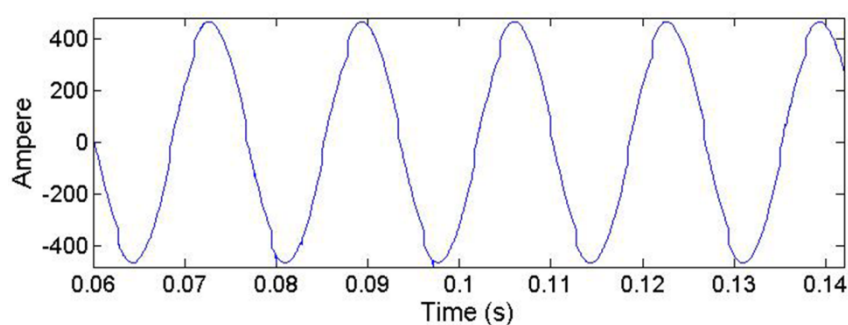
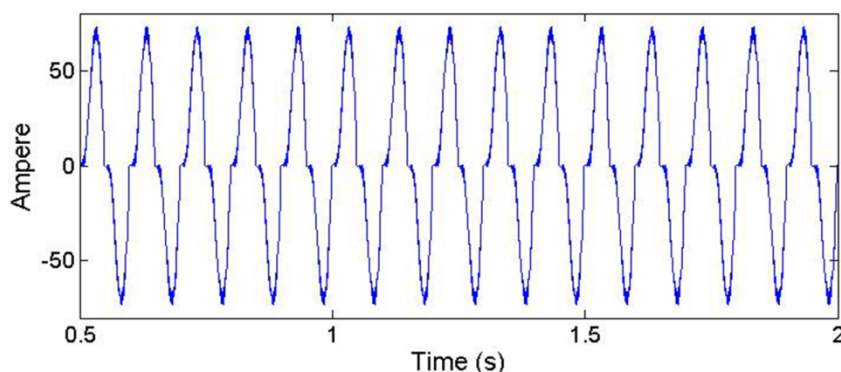


**Figure 2.** Non-characteristic load current caused by the cyclo-converter.



## 2.2. Nonintrusive Energy Monitoring

This subsection details the purpose, benefits, load signature and the process of feature extraction, for the NEM implemented at the PCC. Load monitoring has been used to solve problems in industrial systems and residential households. It is becoming an integral part of performance assessment procedures. As described in Section 1, NEM monitors power generation from distributed generations and individual power consumptions in a microgrid. The benefits of the NEM, for the power utility, include (1) a better understanding of power quality at the PCC; (2) a better understanding of the impact on the reliability of the main grid; (3) the possibility of contract revision between the utility and the microgrid administrators; and (4) identifying problem situations, e.g. malfunctions in protective relays in the main grid.

One of the important steps for NEM is the identification of the signatures of the measured signals at the PCC [3]. The Fourier series coefficients for the currents at the PCC are the signatures used for the purposes of analysis [3–5]. In this paper, FFT-based spectra of harmonic voltages and currents, as well as real/reactive powers at the PCC, serve as signatures for the monitoring of the microgrid.

Nonintrusive monitoring facilities are installed at the PCC. When the signatures of the monitored data are obtained, important features can be further extracted for analysis purposes. The monitoring system assimilates the load features to allow the power utility to make more efficient policies.

## 2.3. Assumptions

As described in Section 2.1, the studied microgrid in this paper is operated by a single customer. To achieve NEM for such a microgrid, this paper makes some assumptions:

- (1) The signatures of signals used to be studied in the microgrid have been properly filtered: The measured signals are attained through CT/PT. The noise-free signals are used for analysis.
- (2) The three-phase system is balanced at the PCC: This paper uses the concept of the CERTS microgrid, so the microgrid must satisfy IEEE Sd. 1547. Any minor imbalance within the IEEE Sd. 1547 limit at the PCC is ignored.
- (3) The number and types of individual loads are known: the individual loads in a microgrid are not like the appliances in a house, where privacy is important. Hence, the types of loads (e.g., 6-pluse converter and cyclo-converter) can be known.
- (4) The different operational levels of individual loads are known: large loads are operated at discrete levels, from their rated (peak) to their off-peak levels, or even the outage state.
- (5) Only energy monitoring is considered: Policy-making, using the results of energy monitoring, is not considered in this paper. The measured/filtered data is continuously sent to a PC in a control center. The proposed hybrid SOFMNN outputs one level of each load and one level of the wind-turbine generator at a time. Because transients caused by load switching only last tens or hundreds of milliseconds, consecutive steady-state levels for each individual load can be determined using the proposed method.

Like most of applications using the neural networks, the parameters of the proposed hybrid SOFMNN must be updated and retrained, using off- and on-line data, if a new load is included or the

system topology is changed. The reason is that the number of output neurons (defined in Section 3.3) is changed.

### 3. The Proposed Method

#### 3.1. Concept of Hybrid Neural Networks

The voltage/current/real power/reactive power, sampled at the PCC, is transformed to the FFT spectrum, including fundamentals, integer (2, 3, 4...) harmonics, sub-harmonics and inter-harmonics. In this paper, it is found that the magnitudes of voltage/current greater than the  $H$ th harmonic, where  $H = 14$ , are small and can be ignored. The components of the FFT spectrum serve as signatures of the sampled voltage/current real power/reactive power (denoted as V, I, P and Q herein), for further signal processing. The identified components are those of 0, 20, 40, 60, 80, 100 and 120...,  $14 \times 60$  Hz. The signatures (FFT spectrum) of the voltage/current real power/reactive power must be further investigated, for at least two reasons:

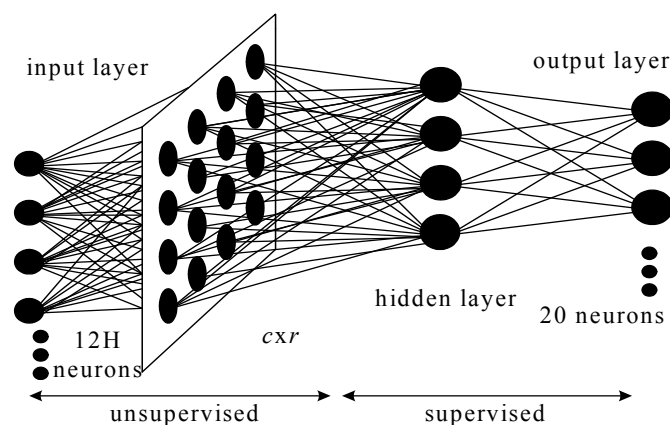
- (1) All components in the FFT spectrum are not equally important. Some FFT components are trivial and should be ignored by further investigation.
- (2) The significant topological structures of the signatures must be arranged to train the supervised neural network. A sequence of ascending frequencies for V, I, P and Q may be inefficient to train the neural network.

Therefore, the proposed SOFMNN firstly extracts the features from the signatures of the FFT spectrums. These features are forwarded to a two-layer supervised neural network. In this paper, the proposed SOFMNN is integrated with the supervised neural network and is called the hybrid SOFMNN.

#### 3.2. Traditional Self-Organizing Feature-Mapping Neural Network

Kohonen proposed a Self-Organizing Feature-Mapping NN (SOFMNN) in 1973 [8], which was an unsupervised NN, using competitive learning. The weighting values for neurons are tuned competitively, according to the inputs. With sufficient training data, the values of the outputs can be represented by a topological structure (one- or two-dimensional space), in terms of inputs. The left-hand side of Figure 3 shows the 2-dimensional topological structure.

**Figure 3.** A Hybrid SOFMNN.



The left-hand side of Figure 3 denotes the traditional SOFMNN. Let the input be:

$$\underline{x} = [x_1, x_2, \dots, x_p]^T$$

and the weight vector for the  $i$ -th output neuron be:

$$\underline{w}_i = [w_{i1}, w_{i2}, \dots, w_{ip}]^T$$

The symbols,  $p$  (identical to  $4 \times 3 \times H$  in this paper) and  $N$ , are the respective numbers of the input and output neurons of the SOFMNN. If:

$$\underline{w}_{i^*}^T \cdot \underline{x} \geq \underline{w}_i^T \cdot \underline{x} \quad i=1,2,\dots,N \quad (1)$$

then the  $i^*$ -th neuron is the winner. Because:

$$\|\underline{x} - \underline{w}_i\| = \left( \underline{x}^T \underline{x} - 2 \underline{w}_i^T \underline{x} + \underline{w}_i^T \underline{w}_i \right)^{1/2} \quad (2)$$

with a minus sign for the term,  $2 \underline{w}_i^T \underline{x}$ , Equation (1) is equivalent to Equation (3) (see Page 346 in [8]):

$$\left\| \underline{x} - \frac{\underline{w}_{i^*}}{\|\underline{w}_{i^*}\|} \right\| \leq \left\| \underline{x} - \frac{\underline{w}_i}{\|\underline{w}_i\|} \right\| \quad i=1,2,\dots,N \quad (3)$$

Equation (3) is generally used in the algorithm. Once the winner has been determined, the weighting vector is updated according to Equation (4) as follows:

$$\underline{w}_i(n+1) = \begin{cases} \underline{w}_i(n) + \eta(n) [\underline{x}(n) - \underline{w}_i(n)], & i \in A_{i^*}(n) \\ \underline{w}_i(n) & i \notin A_{i^*}(n) \end{cases} \quad (4)$$

where  $\eta(n)$  and  $A_{i^*}(n)$  are the learning rate and the winner's neighboring area, respectively. Both of these are functions of the iteration index,  $n$ . More specifically:

$$\eta(n) = \eta_0 \cdot e^{-n}$$

where  $\eta_0$  is the initial learning rate (0.1 herein);  $A_{i^*}(n)$  initially covers 8 neighboring neurons centered at the  $i^*$ -th neuron in a squared area. The number of neighboring neurons decreases to zero when the iterations converge.

### 3.3. Hybrid Self-Organizing Feature-Mapping Neural Network

A traditional SOFMNN only outputs the weightings:

$$\underline{w}_i = [w_{i1}, w_{i2}, \dots, w_{ip}]^T \quad i=1,2,\dots,N$$

The problem is how to utilize the topological structure in the 2-dimensional  $c \times r$  space. Kohonen found the mapped features in the 2-dimensional  $c \times r$  space have characteristics of clustering [8]. He used different labels to identify the original inputs related to the different clusters. Therefore, the identified inputs in different clusters can be applied to different functions. A cluster in our problem means one of 625 classifications ( $5 \times 5 \times 5 \times 5$  at the output layer, see next paragraph). However, several clusters may be very close and hard to be differentiated. Once the SOFMNN algorithmic iterations converge, the given data are grouped into clusters but the number of clusters may not be

equal to 625. Each cluster has a cluster center which has a minimum summation of distances between itself and other data in this cluster. The remaining problem is that which cluster a given input should belong to. To solve this problem, the Euclidian distance between the studied data and each of the cluster centers must be examined. A minimum distance indicates the proximity of the studied input data to the vector of a corresponding cluster center. The above problems cause the SOFMNN not to be used directly.

To avoid these two dilemmas and because of the two reasons depicted in Section 3.1, a traditional unsupervised SOFMNN is cascaded to a 2-layer supervised neural network, as shown in Figure 3. The numbers of neurons in the input, output, second and fourth layers are detailed, as follows:

- (1) The inputs are the FFT components of the V/I/P/Q, measured at the PCC. Two components are also identified, between any two consecutive integer harmonics. For example, the components of 80 and 100 Hz are identified, between  $h = 1$  (60 Hz) and  $h = 2$  (120 Hz). In this example ( $H = 2$ ), the number of the input neurons is  $4 \times 3 \times 2$  (V/I/P/Q with frequencies of 20, 40, 60, 80, 100 and 120 Hz). The term “3” is not relevant to three phases but subharmonics and interharmonics. Let  $H = 14$ . Hence, the proposed hybrid SOFMNN has  $4 \times 3 \times 14$  (= 168) input neurons; that is,  $p = 4 \times 3 \times 14$ , where  $p$  is defined in Section 3.2.
- (2) The second layer is usually a 2-dimensional layer. The size is  $N$  (defined in Section 3.2), equal to  $c \times r$  ( $c$  is the number of neurons in the columns;  $r$  is the number of neurons in the rows). This is discussed in Section 4.
- (3) The third layer is the hidden layer, which is the same as the first layer of the supervised neural network. The number of third layer is approximated by  $(N + 20)/2$ , where 20 is the number of output neurons (see (4) below).
- (4) The number of output neurons in the supervised neural network depends on the numbers of loads and the renewable energy sources. For example, the studied microgrid has one linear load, one converter (rectifier) load, one cyclo-converter load and one wind-turbine-generator. Assume that the loads are operated at their discrete levels (see Section 2.3). Then, there are 20 output neurons (binary bits), which are defined, as follows:
  - (a) 1st–5th bits: 0%, 25%, 50%, 75% and 100% of the rated size for the linear loads.
  - (b) 6th–10th bits: 0%, 25%, 50%, 75% and 100% of the rated size for the converter loads.
  - (c) 11st–15th bits: 0%, 25%, 50%, 75% and 100% of the rated size for the cyclo-converter loads.
  - (d) 16th–20th bits: 0%, 0%–25%, 25%–50%, 50%–75% and 75%–100% of the rated power generated by the wind-turbine-generator.

The generation levels from diesel generators can be considered as dependent variables and determined from the linear loads, converter loads, cyclo-converter loads, and wind-turbine-generators. Thus, no output neurons for the generation levels from diesel generators are required.

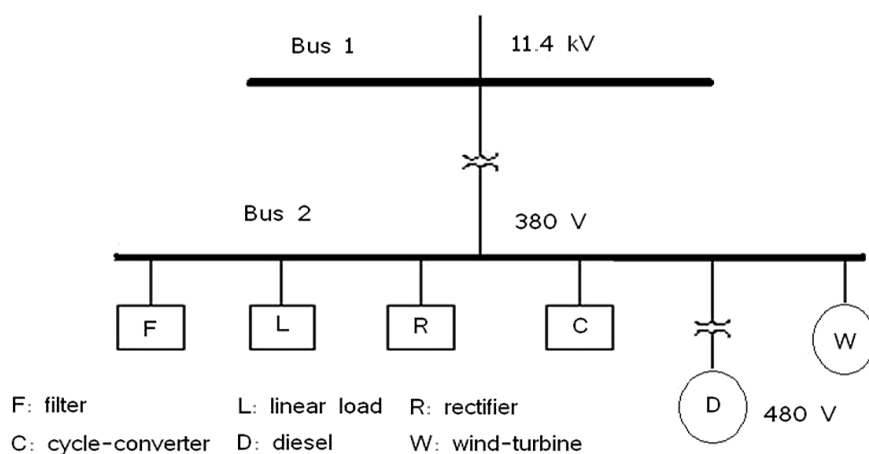
The intermittent nature of the wind power was not considered in this paper because only power generation levels are concerned in an energy monitoring problem, which is relevant to a real-time (on-line) study. A scheduling or planning work requires the probabilistic or stochastic model for the wind power. The objective function for supervised learning (training) is defined as the sum of the mean squared errors between the expected (known) values and computed values.

## 4. Simulation Results

### 4.1. Description of the Studied System

A microgrid, which includes a linear load, a rectifier, a cyclo-converter, a diesel generator and a wind-turbine-generator, was studied, as shown in Figure 4. The short circuit capacity (SCC) is normally 85 MVA and X/R is 7, at the PCC. The ratings for the linear, rectifier and cyclo-converter loads are (41.58 kW + j10 kVAR), 30  $\Omega$  and (40 + j75.36)  $\Omega$ , respectively. In order to compensate for distorted voltages, a damped filter (3.45 kVAR, tuned frequency = 90 Hz, Q factor = 50) is installed at the PCC. The rated capacity and voltage of the diesel generator are 30 kVA and 480 V, respectively. The rated generation for the wind-turbine-generator is 20 kVA. To show the performance of the proposed neural network, a total of 1137 cases were generated, by varying the values of SCC (42.5–85 MVA) as well as linear loads, converter load, cyclo-converter load and wind-turbine output (0%–100% of rating, see Section 3.3). The system is implemented by MATLAB/SIMULINK (please see the Appendix). For training, validating and testing the hybrid SOFMNN 797, 113 and 227 of the 1137 cases were used, respectively. A personal computer, with an Intel Core 2 Duo CPU E4400@2.00 GHz, 3.25 GB RAM was used to study the performance (including required CPU time) of the proposed method.

**Figure 4.** One-line diagram of the studied microgrid.



In the proposed hybrid SOFMNN, the new hidden layer consists of 20 neurons. The second layer is a  $c \times r$  topological structure. The learning rate,  $\eta(n)$ , starts at 0.01 and decays to 0.001. The winner's radius of the neighboring area,  $A_{r^*}(n)$ , is initially set at 3 and decays to 0. After training the unsupervised NN (left side of Figure 3), the supervised NN (right side of Figure 3) is trained, using the frozen weights of the unsupervised NN and then uses the same training set.

### 4.2. Signatures of Voltages and Currents

As described in Section 4.1, 1137 cases were studied. In this subsection, only the voltage and current spectrums for two out of 1137 cases are shown. Figure 5a,b show the FFT spectra of voltage and current for the condition of half linear load, a cyclo-converter at full load, and a rectifier at half

load. Figure 6a,b shows the FFT spectra of voltages and currents for the condition of half linear load, a cyclo-converter at half load, and a rectifier at full load. Note that the fundamental components (harmonic order = 1) of voltages and currents with values of unities in Figures 5 and 6 have been cut to fit the figures. These four figures show that:

- (1) For both voltages and currents, the components of the characteristic harmonic voltages/currents (*i.e.*, 5th, 7th, 11th, 13th) are larger, compared to non-characteristic (inter-) harmonics.
- (2) Many sub-harmonics and DC components of the voltages and currents exist, caused by the cyclo-converter. Some of the sub-harmonics are even larger than those of the characteristic harmonics and inter- harmonics.
- (3) Theoretically, for the voltage and current harmonics, the characteristic harmonics of the 11th and 13th orders are smaller than those of 5th and 7th orders. It is found that a minor parallel resonance occurs, near the harmonics of 11th and 13th orders, in this system.
- (4) The patterns of the FFT spectra for both the voltages and currents at different load levels are different. Therefore, the components of the FFT spectra can be used as signatures for load monitoring.

**Figure 5.** (a) FFT spectrum of voltages (half linear load, cyclo-converter at full load, rectifier at half load); (b) FFT spectrum of currents (half linear load, cyclo-converter at full load, rectifier at half load).

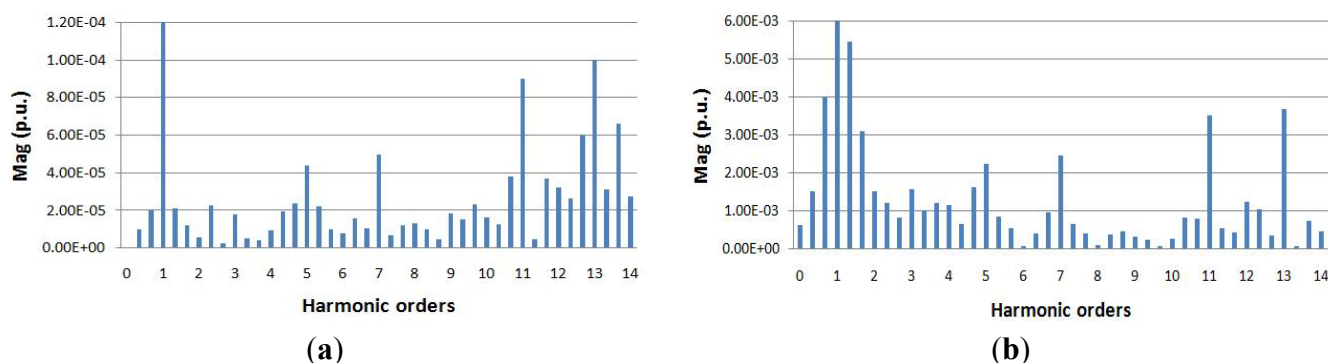
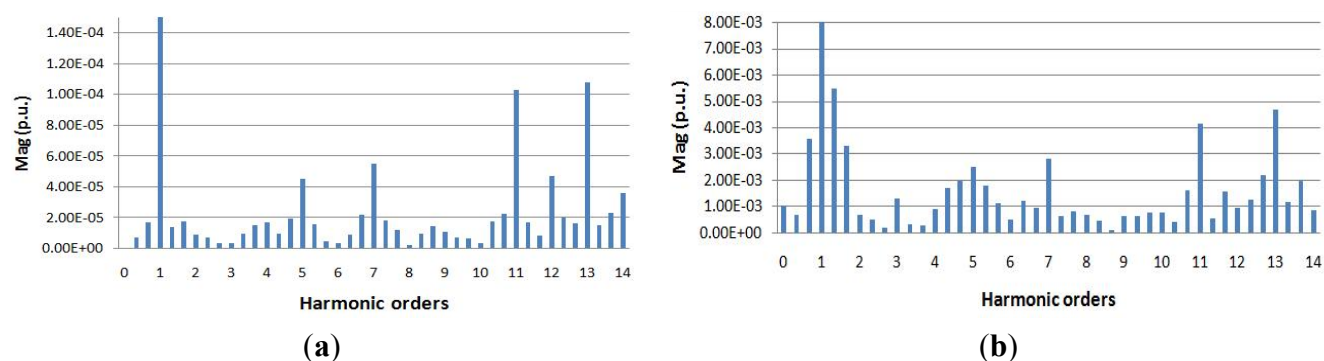


**Figure 6.** (a) FFT spectrum of voltages (half linear load, cyclo-converter at half load, rectifier at full load); (b) FFT spectrum of currents (half linear load, cyclo-converter at half load, rectifier at full load).



### 4.3. Comparative Studies for Different $c \times r$ Topological Structures

In the SOFMNN, the one-dimensional input ( $168 \times 1$  vector) will be mapped into a two-dimensional ( $c \times r$ ) space. Generally, the convergent topological structure in SOFMNN reveals the relation between input neurons. Once the SOFMNN iteration converges, the feature map implies that a winning neuron in the two-dimensional ( $c \times r$ ) space corresponds to its input vector:

$$\underline{x} = [x_1, x_2, \dots, x_p]^T$$

The weight vector:

$$\underline{w}_i = [w_{i1}, w_{i2}, \dots, w_{ip}]^T$$

provides the coordinates of the image of that neuron in the input space. Increasing the value of  $c \times r$  will improve the resolution and accuracy of the proposed method, but also increase the training times. Because the accuracy is more important than the required CPU time in an off-line neural training problem, the values of  $c \times r$  may increase gradually until an acceptable accuracy is attained. It is anticipated that the value of  $c \times r$  should be close to 625 because there are 625 classifications studied in the problem.

Let V, I, P and Q (168 in total) be all of the inputs of the hybrid SOFMNN. Table 1 shows comparative studies for different  $c \times r$  ( $= N$ ) topological structures. As can be seen in Table 1, the accuracy and CPU time increase, when the value of  $c \times r$  increases. The accuracy for the case of  $N = 23 \times 23$  is almost the same as that for the case of  $N = 24 \times 24$ , so  $c \times r = 23 \times 23$  is considered to be the best topological structure, with an accuracy of 99.2%. The required CPU time (19:03) is acceptable, given that the study is conducted off-line.

**Table 1.** Comparative studies for different  $c \times r$  topological structures.

Cases	$c \times r$	CPU (min:sec)	Accuracy (%)
1	$9 \times 9$	2:31	87.6
2	$12 \times 12$	4:25	90.7
3	$15 \times 15$	7:34	96.9
4	$21 \times 21$	15:40	98.8
5	$22 \times 22$	17:28	99.0
6	$23 \times 23$	19:03	99.2
7	$24 \times 24$	20:57	99.2

### 4.4. Comparative Studies for Different Signatures

Table 2 shows the comparative studies among cases considering different signatures while the two dimensional topological structure in the second layer of the proposed method is fixed ( $23 \times 23$ ). It is found that the accuracy for the signatures of voltages (42 in total) is the worst (89.4%), because the fundamental voltages are almost the same and the harmonic voltages are small. The accuracy is the best for the case considering all V, I, P, and Q (99.2%), due to diverse signature inputs to the neural network. The CPU time required for this set of signatures is acceptable for off-line study.

**Table 2.** Comparative studies for different signatures.

Cases	Signatures	CPU (min:sec)	Accuracy (%)
1	V and I (84 in total)	13:21	95.7
2	V (42 in total)	8:41	89.4
3	I (42 in total)	8:21	93.8
4	P and Q (84 in total)	10:55	98.0
5	P (42 in total)	9:02	92.0
6	Q (42 in total)	10:54	95.2
7	V, I, P and Q (168 in total)	19:03	99.2

#### 4.5. Comparative Studies with Traditional Multi-Layer Perceptron

Let V, I, P and Q (168 in total) be all of the inputs of the hybrid SOFMNN. Table 3 shows the comparative studies between existing methods. The 3rd–7th rows of Table 3 show the performance of the traditional, back-propagation (BP)-based neural networks, with different numbers of neurons (20, 40, 80, 110 and 120) in the hidden layer. The last row in Table 3 illustrates a multi-layer perceptron that employs genetic algorithms (GA) to minimize the mean-squared error in the output neurons [7].

BP-based NNs have the fastest convergence, but the lowest accuracy. The greater the number of neurons in the hidden layer, the more accurate is the BP-based NN, as can be seen in Table 3. However, an accuracy of 96.6% represents the practical limit.

The GA is capable of attaining a global optimum, so a GA-based NN has a better accuracy, at 97.8%, compared with that obtained with a BP-based NN. However, a GA-based NN requires more than 14 hours, to train the NN. In this study, the population size, crossover rate and mutation rate are 50, 0.9 and 0.01, respectively.

The proposed hybrid SOFMNN has the best accuracy, at 99.2%, and an acceptable CPU time of 20 minutes and 57 seconds. Compared with the BP-based NN, the proposed method obviously requires more CPU time because the inputs of the cascaded 2-layer supervised neural network of the proposed hybrid SOFMNN are the  $24 \times 24$  features. However, the number of input neurons of the BP-based NN is still 168. It is unfair to increase the number of neurons in the hidden layer of the BP-based NN to  $24 \times 24$  (or  $23 \times 23$ ) for the sake of comparison because the practical number of neurons in the hidden layer is only 94 (*i.e.*,  $(168 + 20)/2$  herein). It is also impractical to increase the number of input neurons of the BP-based NN to  $24 \times 24$  (or  $23 \times 23$ ) because at most 168 signatures are available.

**Table 3.** Comparative Studies between Different Methods.

Methods	CPU time	Accuracy (%)
The proposed SOFMNN	20:57	99.2
BP-based NN of 20 neurons in hidden layer	0:39	92.9
BP-based NN of 40 neurons in hidden layer	1:10	94.0
BP-based NN of 80 neurons in hidden layer	2:11	95.5
BP-based NN of 110 neurons in hidden layer	2:50	96.5
BP-based NN of 120 neurons in hidden layer	3:19	96.6
GA-based NN [7]	14:38:00	97.8

## 5. Conclusions

This paper proposes a new method to conduct nonintrusive energy monitoring for microgrids, based on the FFT and a hybrid SOFMNN. The advantages of the proposed method can be summarized as follows: (1) the spectrum of the FFT is used to determine the signatures of non-characteristic and non-periodic signals; (2) in addition to the voltages and currents, real and reactive powers also serve as signatures and greatly improve the accuracy; and (3) the hybrid SOFMNN can determine the features of the FFT components, which lead to a greater accuracy than existing methods.

The simulation result from a microgrid operated by a single customer shows the practicability of the proposed method. Future studies will include an investigation of different signatures (e.g., wavelet transform) and other renewable energy sources (e.g., solar PV).

## Acknowledgments

This work was supported in part by the Institute of Nuclear Energy Research (INER, Longtan 32546, Taiwan) under Grant NL1000250, NSC 101-3113-P-042A-001 and NSC 99-2632-E-033-001-MY3.

## References

1. UNFCCC. *Kyoto Protocol to the United Nations Framework Convention on Climate Change*; United Nations: Kyoto, Japan, 1997.
2. IEEE Standards Coordinating Committee. *IEEE Application Guide for Interconnecting Distributed Resources with Electric Power Systems, IEEE Standard 1547™*; IEEE: New York, NY, USA, 2011.
3. Hart, G.W. Nonintrusive appliance load monitoring. *Proc. IEEE* **1992**, *80*, 1870–1891.
4. Leeb, S.B.; Shaw, S.R.; Kirtley, J.L., Jr. Transient event detection in spectral envelope estimates for nonintrusive load monitoring. *IEEE Trans. Power Deliv.* **1995**, *10*, 2000–2010.
5. Cole, A.; Albicki, A. Nonintrusive identification of electrical loads in a three-phase environment based on harmonic content. In *Proceedings of 17th IEEE Instrumentation and Measurement Technology Conference*, Baltimore, MD, USA, 1–4 May 2000; pp. 24–29.
6. Cox, R.; Leeb, S.B.; Shaw, S.R.; Norford, L.K. Transient event detection for nonintrusive load monitoring and demand side management using voltage distortion. In *Proceedings of 21st IEEE PES Applied Power Electronics Conference and Exposition*, Dallas, TX, USA, 19–23 March 2006; pp. 1751–1757.
7. Chang, H.H.; Yang, H.T. Apply a nonintrusive energy management system to economic dispatch for cogeneration system and power utility. *Appl. Energy* **2009**, *86*, 2335–2343.
8. Bose, N.K.; Liang, P. *Neural Network Fundamentals with Graphs, Algorithms, and Applications*; McGraw-Hill Inc.: New York, NY, USA, 1996.
9. Hong, Y.Y.; Chang, H.L.; Chiu, C.S. Wind power forecasting using simultaneous perturbation stochastic approximation (SPSA) algorithm and neural network with fuzzy inputs. *Energy* **2010**, *35*, 3870–3876.
10. Zhou, D.Q.; Annakkage, U.D.; Rajapakse, A.D. Online monitoring of voltage stability margin using an artificial neural network. *IEEE Trans. Power Syst.* **2010**, *25*, 1566–1574.

11. Gutierrez-Martinez, V.J.; Cañizares, C.A.; Fuerte-Esquivel, C.R.; Pizano-Martinez A.; Gu, X.P. Neural-network security-boundary constrained optimal power flow. *IEEE Trans. Power Syst.* **2011**, *26*, 63–72.
12. Mehraeen, S.; Jagannathan, S.; Crow, M.L. Power system stabilization using adaptive neural network-based dynamic surface control. *IEEE Trans. Power Syst.* **2011**, *26*, 669–680.
13. Kim, J.Y.; Kim, H.M.; Kim S.K.; Jeon, J.H.; Choi, H.K. Designing an energy storage system fuzzy PID controller for microgrid islanded operation. *Energies* **2011**, *4*, 1443–1460.
14. Xiao, Z.; Li, T.H.; Huang, M.; Shi, J.H.; Yang, J.J.; Yu, J.; Wu, W. Hierarchical MAS based control strategy for microgrid. *Energies* **2010**, *3*, 1622–1638.
15. Papadimitriou, C.N.; Vovos, N.A. Transient response improvement of microgrids exploiting the inertia of a doubly-fed induction generator (DFIG). *Energies* **2010**, *3*, 1049–1066.
16. Lasseter, R.H.; Eto, J.H.; Schenkman, B.; Stevens, J.; Vollkommer, H.; Klapp, D.; Linton, E.; Hurtado, H.; Roy, J. CERTS microgrid laboratory test bed. *IEEE Trans. Power Deliv.* **2011**, *26*, 325–332.
17. Pelly, B.R. *Thyristor Phase-Controlled Converters and Cycloconverters: Operation, Control, and Performance*; Wiley-Interscience: New York, NY, USA, 1971.

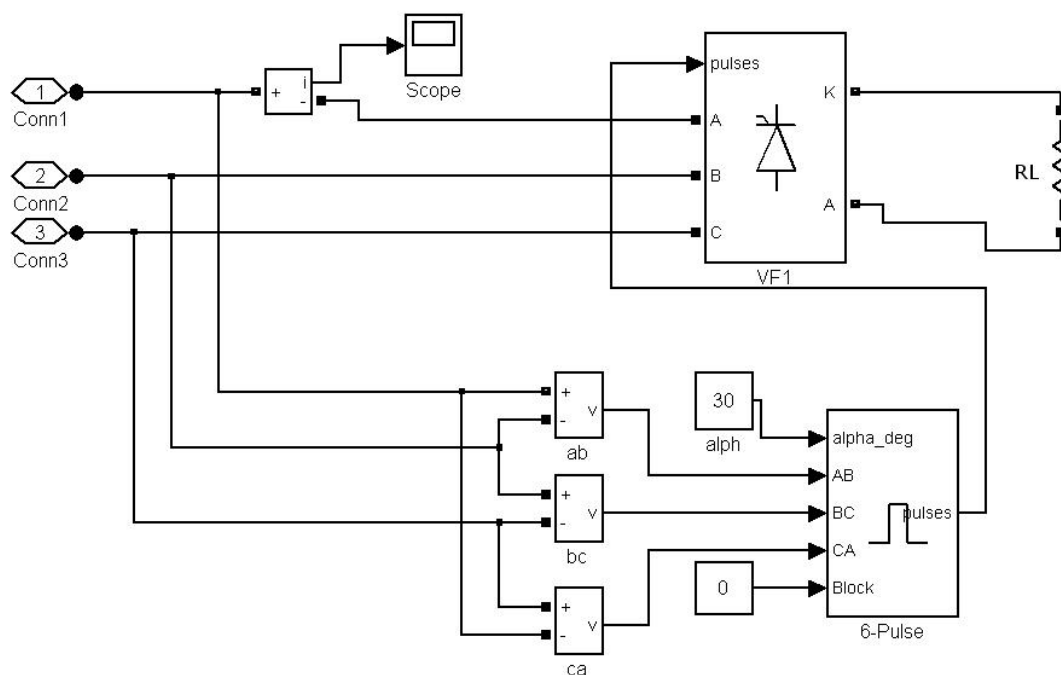
## Appendix

This appendix provides the description of the elements of the studied microgrid in this paper.

### A1. Rectifier

Figure A1 illustrates the rectifier implemented by SIMULINK. Its corresponding instantaneous load current was shown in Figure 1. The block with a thyristor symbol is a function which is able to transfer three-phase voltages to a DC voltage.

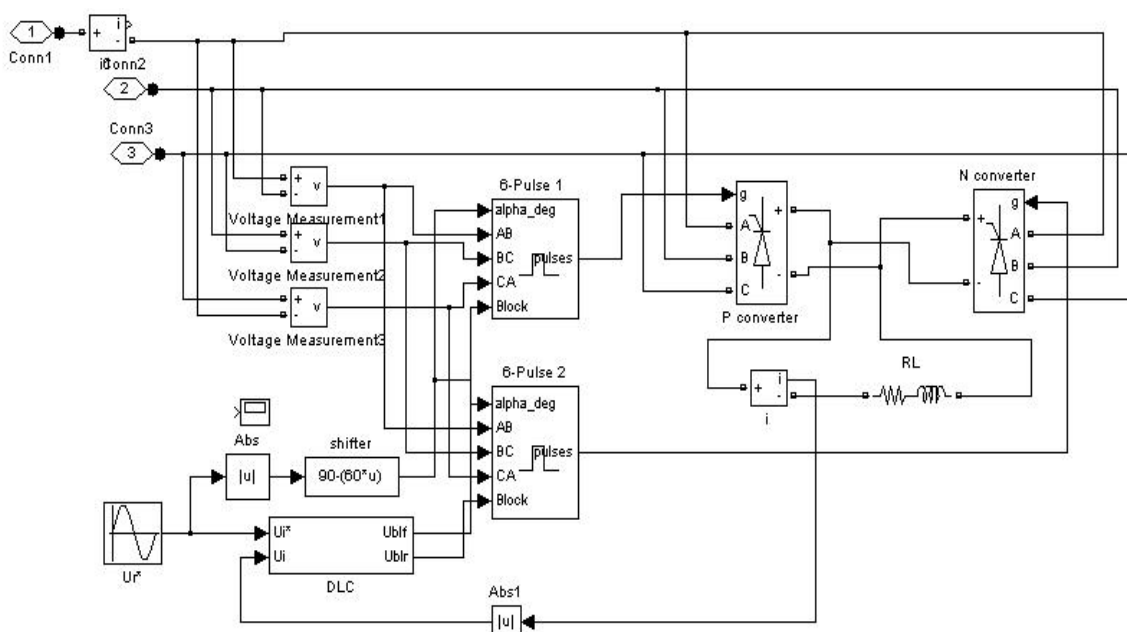
**Figure A1.** Rectifier implemented by SIMULINK.



## A2. Cyclo-Converter

Figure A2 shows the cyclo-converter implemented by SIMULINK. The corresponding non-characteristic load current was given in Figure 2. The cyclo-converter consists of a digital logic controller (DLC), and 6-pulse P and N converters. The DLC is composed of a voltage detector and logic and time delay circuits. The load currents from the cyclo-converter are non-characteristic and include inter-harmonics (whose harmonic orders are within two consecutive integers) and sub-harmonics (components with frequencies smaller than the fundamental frequency).

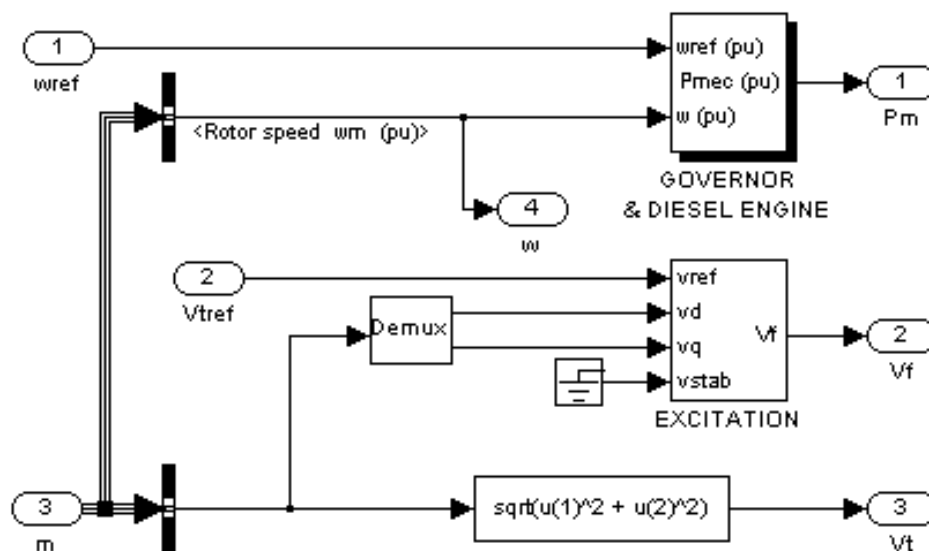
**Figure A2.** Cyclo-converter implemented by SIMULINK.



## A3. Diesel Generator

The diesel generator is a synchronous generator with a diesel engine unit (SD). The SD excitation is performed by the standard excitation block provided in the machine library of SIMULINK. The diesel engine and governor system are modeled by a SIMULINK block. Figure A3 shows the governor/diesel engine and excitation implemented by SIMULINK. This is an existing blockset provided in SIMULINK. The details of block “governor & diesel engine” can be found in SIMULINK Tutorial Session 5. The block “excitation” implements an IEEE type 1 voltage regulator combined to an exciter. The output of this block is the field voltage in p.u. applied to the input of a synchronous machine. The direct- and quadrature-voltages ( $v_d$  and  $v_q$  in the block) are measured from the synchronous machine.

Figure A3. Governor/diesel engine and excitation implemented by SIMULINK.



#### A4. Wind-Turbine Generator

The generator is an asynchronous machine which is modeled in a d-q frame. The generator is connected to the bus with a shunt capacitor for compensating the reactive power. The mechanic torque of wind turbine is set up by a 2-D linear interpolation considering the wind speed and rotor speed as independent variables.

© 2012 by the authors; licensee MDPI, Basel, Switzerland. This article is an open access article distributed under the terms and conditions of the Creative Commons Attribution license (<http://creativecommons.org/licenses/by/3.0/>).